Creating Implants from Allograft Bone using Subtractive Rapid Prototyping

Matthew C. Frank, PhD, Ashish Joshi, MS, Shuangyan Lei, MS
Department of Industrial and Manufacturing Systems Engineering
Iowa State University, Ames, IA, USA
Donald D. Anderson, PhD, Yuki Tochigi, MD, PhD, and Thomas D. Brown, PhD
Department of Orthopaedics and Rehabilitation
The University of Iowa, Iowa City, IA, USA

Abstract

This research involves the development of rapid manufacturing for bone implants using human allograft bone in a Subtractive Rapid Prototyping process. Using CT-derived CAD models of missing bone due to high energy trauma or tumor resection, surgical reconstruction could be improved with custom rapid implants made from natural bone. The bone "stock" material is of arbitrary shape and material distribution in the form of frozen donated cadaveric bones. Each is unique in shape and has highly anisotropic material properties; likewise for each final bone implant geometry and its material distribution. This work utilizes a PLY input file, instead of the more common STL, using color texture information that can be utilized for advanced process planning depending on whether the surface is fracture, periosteal or articular in origin. Moreover, we present a new PLY assembly model, called the *Matryoshka* model, where successively nested PLY files are used to designate changing material distributions in the donated bone; a method that could also aid in the use of multi-material additive RP systems. Using color *Matryoshka* models and their subsequent color slice files; this work presents novel solution methods for the selection of implant harvesting sites and automated process planning for the physical rapid prototyping process. Early implementations using bone surrogate materials will be presented.

Introduction

Segmental bone defects pose major challenges for orthopedic management. Whole sections of bone are oftentimes missing or must be surgically removed during the treatment of disease or trauma. In order for the bone as a whole to function properly, it is essential that the defect be filled with an implant that is both mechanically and biologically stable. Towards that end, shaping the implant from clinically relevant material can be challenging. Frequently, the surgeon sculpts these implants by hand to fit the defect, during surgery. That task is prone to inaccuracies that can lead to complications, particularly for joint fractures, where a poorly filled bone defect can alter the joint mechanics, compromise implant fixation stability and ultimately cause the joint to degenerate. The field of rapid prototyping now offers several methods for creating implants from solid or porous materials, and from bioactive scaffolds.

This paper presents the novel application of advanced Subtractive Rapid Prototyping (SRP) methods to the field of orthopedics [1,2]. The work was performed at the Iowa State University (ISU) Rapid Manufacturing and Prototyping Laboratory (RMPL), in collaboration with the Orthopedic Biomechanics Laboratory at the University of Iowa (UI). The objective of this research was to develop algorithms that would facilitate machining of patient-specific bone implants from frozen donor cadaveric bones (allografts) as the stock material. Implant made from allografts could have a unique density distribution throughout its volume. Having a density distribution on the implant similar to the one at fracture site could allow the parent bone to integrate with the implant effectively compared with other bio-implants. Also, in order to facilitate effective healing, it is necessary for the implant to maintain its initial fixation stability. This could be achieved by providing surface specific characteristics (textures) on the machined implants. Hence the algorithms designed in this research aid in choosing an appropriate implant location within the donor bone to impart unique density distribution and choosing process parameters that facilitate implant machining with customized surfaces (textures) to increase the implant's fixation

stability. The CAD geometries of segmental defects (residual voids/implants) were extracted and designed using fracture reconstruction planning software developed at the University of Iowa (*FxRedux*) [3,4] to analyze patient CT data. The corresponding custom defect filling implants were fabricated using an SRP technique called CNC-RP at Iowa State University.

The clinical need: custom-fit allograft bone for implantation

Even in the current era of sophisticated bone grafting procedures, advanced synthetic biomaterials and bioactive/tissue engineered implants, refined capabilities for restoring soft tissue coverage, and highly evolved distraction osteogenesis techniques [5], treating segmental bone defects presents a major challenge. To date, most attention in this area has focused on mid-shaft long bone defects, where the principal reconstructive objective is to achieve bone healing with nominal preservation of limb length and alignment. While shape matching between the graft and the recipient site is always desirable in principle, many mid-shaft fractures are relatively forgiving in that regard. Various other bone defects, by contrast, place a much higher premium on close geometrical matching of the graft. For example, bone defects associated with severe articular or peri-articular fractures (i.e., fractures near a joint such as the knee or hip) require a substantially higher degree of reconstruction accuracy than is the case for the mid-shaft defects, owing to the need for stable, congruous articulation of the joint surface. Bone healing of an articular fracture in other than closely anatomic position predisposes the joint to secondary arthritis, a major contributing factor to poor outcomes, whose morbidity frequently approaches that of amputation [6].

At the local macroscopic level, all fractures possess individual geometric signatures. Current synthetic implant or grafting strategies for achieving healing of segmental defects offer only limited opportunity to address individualized defect geometry, since they have evolved mainly for situations (mid-shaft defects) where close reconstruction of local geometry is not particularly critical. Using conventional methods, there has to be primary reliance on fixation hardware to hold the respective bone surfaces in the desired nominal apposition, with the implant or graft making at best local spot contact with the recipient bone, and with appreciable gaps existing across much if not most of the intended-union interfaces. Even with the most advanced contemporary fixation in the hands of highly trained orthopaedic traumatologists, comminuted peri-articular fractures (especially in the presence of segmental defects) pose a severe biomechanical challenge, that often is not well resisted by usage of conventional bone grafts [7]. Virtually all contemporary synthetic implant materials, all tissue engineered defect-filling constructs, and especially all variants of bone grafts would have better prospects for achieving optimal outcome, if they began from a condition of closely fitting the local geometry of the recipient bone surface(s).

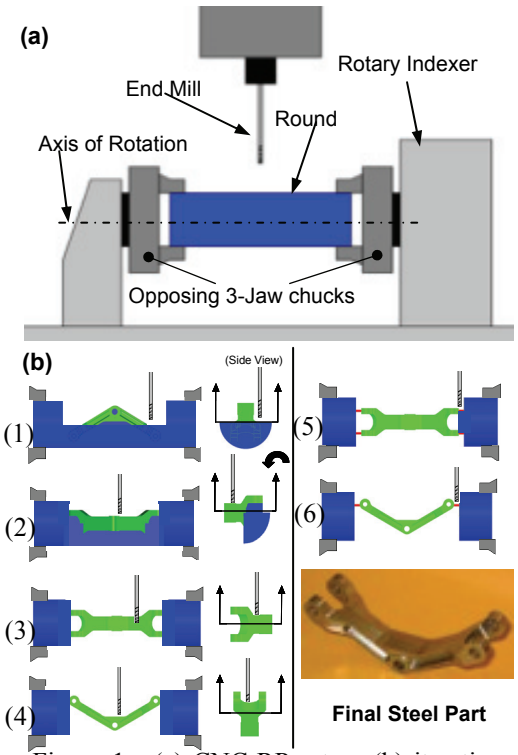

Figure 1 - (a) CNC-RP setup; (b) iterative steps of layer based toolpath planning from multiple angles, using sacrificial supports to fixture the part to the remaining stock

Rapid manufacturing using CNC-RP

CNC-RP is a fully functional Subtractive Rapid Prototyping (SRP) process using a standard 3-axis CNC milling machine with a 4th axis for multiple setup orientations. The CNC-RP approach features completely automated fixture planning, tooling and setup planning, including generation of NC code

for creating a part directly from a CAD file [1,8,9]. The use of a rotation axis eliminates the need for re-clamping of the part, a common task in conventional fixturing methods [10,11]. For each orientation, all the visible surfaces are machined while a set of sacrificial supports keeps the part connected to the uncut end of the stock material. Once all the operations are complete, the supports are severed (sawed or milled) in a final series of operations, and the part is removed [12]. The setup and steps to this process are illustrated in Figure 1. The manufacturing of biomedical implants provides a challenge very well suited for CNC-RP, especially due to the fixturing issues and the need for specialty materials (in particular, human allograft bone). Figure 2 shows a fragment from a human tibia which was reverse-engineered from a CT scan and then rapid-machined from clinically relevant materials using the CNC-RP process.

Bone Implant Harvesting

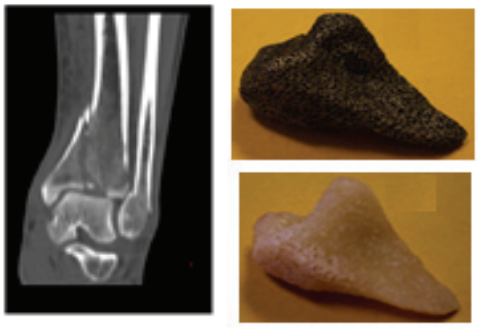

Figure 2 - Implant prototyping from CT scan to machined porous metal (Trabecular Metal™) and native bone (bovine)

The authors have been developing methods to harvest custom bone implants from donor bone, with implant geometries derived from CT scanning of patients' bones [2]. In order to effectively create patient-specific implants from a donor bone, one needs to find the optimal location within the donor bone from which to harvest the implant. A challenge in this approach is that donor bone is unlike a homogeneous artificial bone material, where the implant could be harvested from anywhere within the stock material volume. Natural bone has heterogeneous internal structure, and the site of implant harvest needs to respect the realities of internal bony density distribution; not all harvest locations that are geometrically feasible will be clinically suitable. Figure 3(a) shows a cross-sectional view of a femur bone, showing the spongy, low density trabecular bone in the middle, versus the high-density cortical bone on the outside. A surgical bone implant might need to have a bone material density that is highly, or almost entirely cortical bone, or it may need a particular distribution of densities, or it may simply need to try to match the general gradient directions. Regardless, there needs to be an efficient way to represent the complex material properties given piece of such "stock material".

Figure 3 – Comparison of bone to stacking doll models, (a) A cross-sectional view of a femur bone, *Matryoshka* shell model; (b) Set of Matryoshka dolls, in order of size and (c) Cut-away view of nested *Matryoshka* dolls

To meet this challenge, we propose the idea of a *Matryoshka* shell model as a way to describe the bone density distribution, using discrete regions generated from CT image data. As a simple example, Figure 3(b) shows a set of Matryoshka nested dolls. The salient characteristic of Russian nesting dolls is that the size of each nested doll decreases in order to place one inside the other, as shown in Figure 3(c). Although models generated from bones will not exactly follow the monotonically decreasing regions of these dolls, the general concept of nested shells is the underlying principle.

The Matryoshka Shell Model

The task of defining density function is not trivial, since bones have a complex heterogeneous structure. There have been numerous research efforts to model the density of bone. The Hounsfield Unit (HU), which quantifies the X-Ray attenuation, indicates the varying bone density levels; High HU corresponds to high density, and vice versa. HUs are also associated with grayscale of the CT slice image, which carries intensity information. By setting threshold HU values, pixel values below given threshold values can be set to be pixels-of-interest, while HU values above the threshold values can be set to be background pixels. Figure 4 shows an example of distinguishing pixels of interest from a CT slice image, using the HU threshold method divided into 5 different regions bounded by different contours. When each increasing contour shell is created, it is assumed that the pixels within that region have a common singular HU around the thresholding value. Hence, the continuous bone density function exhibited on the CT slice can be discretized into a step function. The 3D Matyroshka model created by iterative thresholding operation on a series of CT slices and stacking them together is saved as a single PLY file. This PLY file can be used for determining the location in the donor bone from which the implant can be machined. An example of a Matryoshka model from a human Tibia is shown in Figure 5 with five shells; the innermost medullary cavity (Shell 1), low-density cancellous bone (Shell 2), high-density cancellous bone (Shell 3), cortical bone (Shell 4), and the bone outer surface (Shell 5).

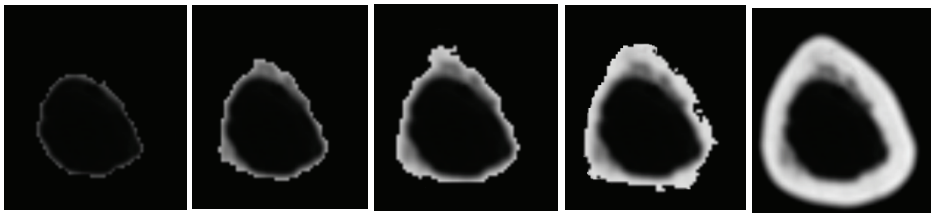

(a) (b) (c) (d) (e)

Figure 4 - Distinguishing the pixels of interest from the CT slice image by the HU threshold method, (a) HU ≤1203; (b) HU ≤ 2277; (c) HU≤ 2768; (d) HU≤ 2982; (e) HU ≤ 3140

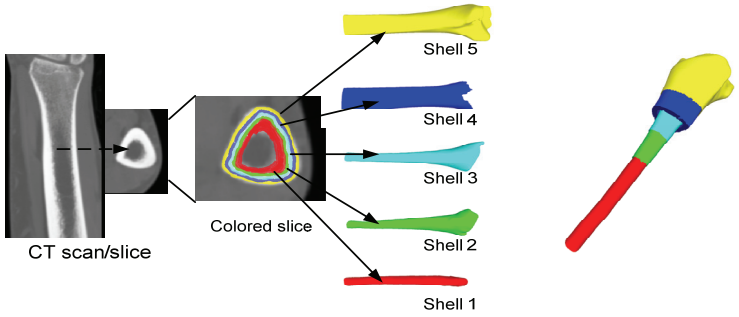

(a) (b) (c) (d)

Figure 5 - Matryoshka model of the human tibia, (a) CT Scan and slice; (b) view of colored cross-sectional geometry; (c) 5 shells generated from the medullary canal to outer bony surface; and (d) cut-away view of an assembled final model

Using a Matyroshka model for bone implant harvesting

The goal of the Matryoshka model is to enable automated searching for a suitable harvest site within a donor bone from which to rapid machine the desired implant. Although the space can appear to have infinite solutions for positioning and orienting the implant, we wish to reduce the degrees of freedom for searching based on known characteristics of human long bones. Usually human *long bones* (femur, tibia,

humerus, etc) are attractive as donor bones. If shape similarity is considered between a long bone and a cylinder, a long bone generally exhibits increasing density away from the axis radially, or the medullary canal. This gives a basis for defining the "center line" of the bone. Before initiating a harvesting search within the donor bone, it is first important to align the "center lines" or axes of the patient bone and donor bone. Thus, the density distributions in the implant and the donor bone would generally align radially along the same axis. When one traverses a set of cylindrical coordinates in the donor or patient bone space, the gradient directions will generally align (i.e. moving away radially will increase density in both, and vice versa). Hence, our simplified harvesting search involves implant rotation about and translation around the center line in the donor bone space.

Creating a discretized slice model

Before the iterative search begins, the Matryoshka model is sliced about the center line. The colored slice can be considered as a boundary; the region within each color boundary represents its density and is given one specific value. In this manner, all elements contained between two adjacent shells are set to the same value, other than the first shell which contains the medullary canal and this is not a feasible region for bone harvesting. As shown in Figure 6(b), values *a*, *b*, *c*, and *d* represent the bone densities from different regions in the slice model. Next, a spider cell structure is used to discretize each slice into a grid of sectors about the *Z*-axis, with an interval angle α, and with each sector further divided by grid elements with interval *h*, as shown in Figure 6(c). Each grid element is assigned a specific value indicating the density of the region encompassed by the corresponding grid element. In general, smaller α and *h* will result in a more accurate and finer discretization structure, but at the expense of increased computation time (The grid spacing for both α and *h* are shown excessively coarse in Figure 6(c) for clarity; in practice, they are 1-5˚ and 1-3mm, respectively).

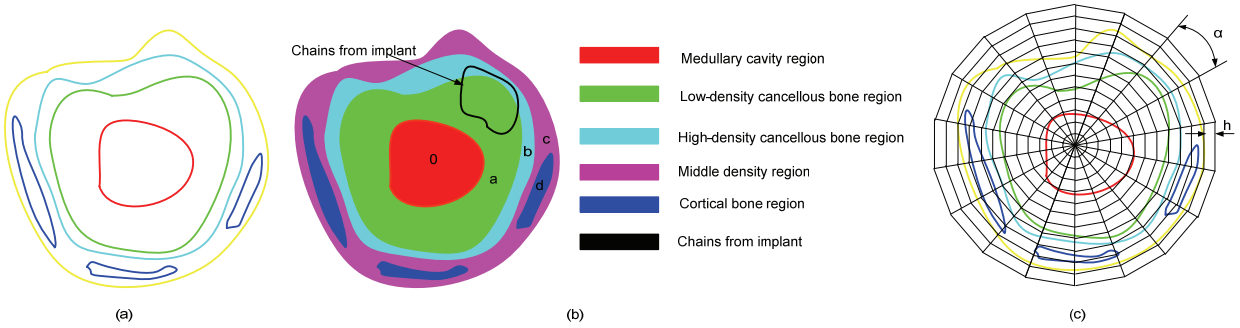

Figure 6 - (a) One cross-section from a Matryoshka shell model; (b) Color mapping for different density regions; (c) Discretized density regions.

For each slice, an array is used to indicate the presence of the shell in the grid structure. If any side of the grid element intersects the chain, a specific value is assigned to represent the existence of a specific shell in that element at a specified density, with values of *a*, *b*, *c*, *d* used to represent the existence of Shell 2, Shell 3, Shell 4 and outer surface Shell 5, respectively. If no shell intersects any grid element, a value of 0 is assigned to the corresponding element in 2D array as shown in Figure 7(b).

Since all grid elements that fall within the surface boundaries of the bone will be assigned to one of the specific density regions, those grid elements temporarily indexed in the array with value of 0 need to be modified to represent the density correctly. For example, after filling in the 0 elements of the array, the updated row of the array is as shown in Figure 7(c).

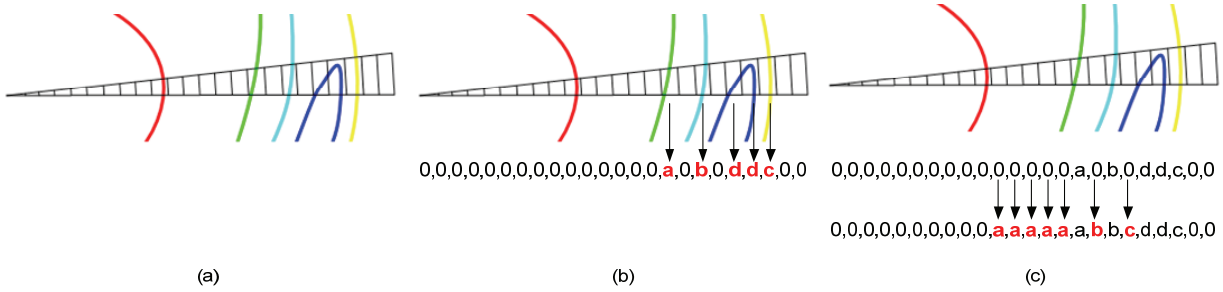

Figure 7 - Section chains intersecting the grid elements, (a) One spider cell region, (b) Shell boundary detection, and (c) Element fill

Density score and similarity score calculation

The goal is to assign a quantitative score of "goodness" for a candidate location for bone implant harvesting. This will be focused on the density of the implant, regardless of whether the preference is simply for high overall density, or for a highly similar distribution of densities between donor and patient. To begin, after discretizing the slice model into the grid structure and assigning a density value in each element, the area of each element is determined based on parameters α and h. To calculate the overall effectiveness score for the entire provisional implant position, density metrics are calculated for each chain of each slice for the entire implant, as follows:

Let N be the total number of slices for the implant, for i slices from 0 to N-1. Let j , ranging from 0 to 3, represent the four bone density regions. Then, let S_{ij} indicate the area of the different density regions j on slice i. Recall that the density regions 0, 1, 2, 3 represent the range from low-density cancellous bone region to the highest density cortical bone region. Then, the area matrix S is normalized by:

$$S_{ij} = \frac{s_{ij}}{\sum_{i=0}^{N}\sum_{j=0}^{3} s_{ij}} \tag{1}$$

i=0, 1,…(N-1) (slice), j = 0, 1,…, 3 (region)

Finally, the density score is calculated by:

$$Density\ score = \sum_{i=0}^{N-1}\sum_{j=0}^{3}(S \times A^T) \tag{2}$$

$$A = [a, b, c, d] \tag{3}$$

Using the same procedure, the normalized area matrices S and S' are calculated for the donor bone and patient bone, respectively. The similarity score is then calculated by:

$$Similarity\ score = \sum_{i=0}^{N-1}\sum_{j=0}^{3} abs(S_{ij} - S'_{ij}) \tag{4}$$

These two scores, *Density* and *Similarity*, can then be used independently or together, to calculate the effectiveness of a provisional harvest site. Whereas Density is an aggregate score for the entire implant, Similarity is evaluated slice by slice. Hence, although one could achieve a high overall density score by having some portion of the implant gain density at the expense of another portion losing density; the Similarity score will be affected more locally.

Conceptually, the simplest approach is to conduct an exhaustive search of the entire donor bone space, in order to determine the optimal location for the harvested implant. This exhaustive search involves rotating the implant about the Z-axis, and translating the implant up and down in the Z-axis direction, while moving the implant near to or far away from the Z-axis radially. In other words, the implant is moved at

the granularity of the spider grid structure, throughout the entire donor bone space. For each iteration, the Density and Similarity are calculated, and then both values are normalized. In our current implementation, a final attractiveness score is calculated based on a weighted function of the aggregate "goodness" of each feasible solution.

$$Max\ \{\alpha \times Normalized(density\ score) + \beta \times Normalized(similarity\ score)\} \quad (5)$$

Here α and β are coefficient weights on the importance of Density and Similarity, values which can be assigned by the surgeon, radiologist, tissue bank technician, etc.

Once the search is complete, we effectively know "where" we would like to machine the implant from the donor bone. Using CNC-RP, we currently have solutions for automatically machining a part from simple stock, with homogenous properties. The problem now is that we are faced with a "part", the implant, where its functionality, both density and surface characteristics can have significant impact on biocompatibility and performance. To this end, the following section illustrates how one can find surface specific machining operations based on a colored polygonal model; allowing us to deliver custom surfacing on the implants without human intervention in process planning.

Process planning for calculating sub-surface specific orientations

After determining the location for harvesting the implant, setup orientations can be calculated for machining the implant with customized surfaces. In previous work for CNC-RP process planning, it was only deemed necessary that the entire surface of the part model be machined after all setup orientations were completed. This problem of calculating the set of setup orientations for machining the entire part is classified as a Set Cover problem, where the whole surface of the part model visible in the range of 0° to 360° is included in the universal set (Figure 8). The algorithms designed for the CNC-RP ensure that each portion of the part surface visible in the range of 0° to 360° is machined from at least one setup orientation from the solution set. Referring back to the CNC-RP introduction in Figure 1, this basically entails determining the setups for the machining process about the rotary axis, or number of times we need to stop and deploy a set of toolpaths. Due to the lack of sub-surface identification on the STL file, the previous algorithms for calculating setup orientations were designed to target the entire model geometry, but do not create different finishes on each sub-surface. Instead, if one could pass information about different surfaces on the bony anatomy of the implant then customized machining operations could be implemented for each. In this work, color PLY files are used to designate surfaces as Fractured, Articular, or Periosteal in origin, passing this color of the facets onto the slice polygons (Figure 9). The basic Set Cover approach is used here, but with the significant difference of achieving set cover for each sub-surface individually, rather than for the entire model. Thus, in order to target individual sub-surfaces, setup orientations have to be chosen such that they are aimed at sub-surfaces individually (Figure 10) rather than at multiple sub-surfaces together. In this work, setup orientations specific to the articular/periosteal/fracture sub-surfaces are designated with subscript $\boldsymbol{\theta}_{a/p/f}$. The process planning algorithms developed for choosing sub-surface-specific setup orientations consider the primary variables of 1) Surface Visibility (SV), 2) Surface Reachability (SR), and 3) Normal Deviation (ND) (Deviation of a candidate setup orientation from the average sub-surface normal).

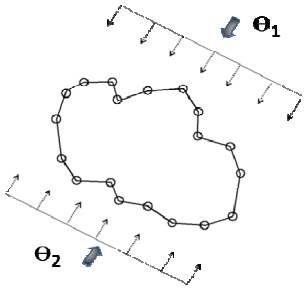

Figure 8 - Setup orientations using STL

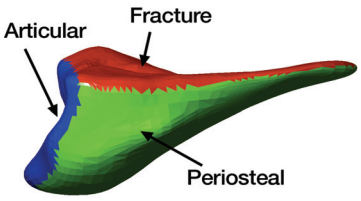

Figure 9 – Color PLY file for implant geometry

Sub-surface Visibility (SV)

Visibility is a necessary condition for a given sub-surface to be machined by CNC-RP. For example, if the objective is to machine the articular sub-surface, a setup orientation from which articular sub-surface is visible must be chosen for machining it. Hence the primary aim would always be to maximize the visibility of the sub-surface for which setup orientation(s) is being chosen.

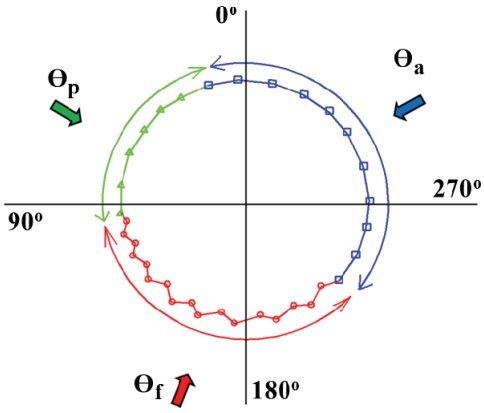

Figure 10 - Setup orientations targeting individual sub-surfaces

Sub-surface Reachability (SR)

In order to ensure that entire part can be machined, it is necessary that every visible sub-surface on the part also be reachable from at least one orientation. For example, there could be an instance where a certain percentage of a sub-surface is visible from a given orientation, but is not reachable because of inadequate tool length. Thus, the total reachable perimeter is calculated by comparing the maximum available tool length against the perpendicular distance from each visible point to the tangent line at the given orientation (Figure 11). Hence, the aim here is to maximize the Surface Reachability while choosing setup orientations.

Normal Deviation(ND)

One of the factors to be considered is the texture directionality created on a sub-surface. For example, in order to have stable implant fixation, it is desirable that we can impart a textured surface onto it to allow better bite into the existing site. This ability increases as we can align toolpaths with a more normal apposition to the desired surfaces. Hence, minimizing the Normal Deviation (ND) is sought (Figure 12). This is not only true when attempting a rough surface, but also for a smooth surface, where an increase in ND generally increases the scallop height. Ironically, the same is needed whether an intentionally rough or smooth surface texture; hence, the aim here is to have *minimal* Normal Deviation (ND) for setup orientations.

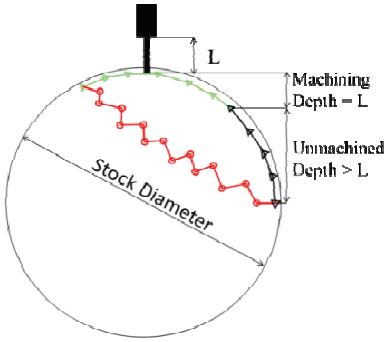

Figure 11 - Surface Reachability
Tool Length L < Depth D,

Goodness Measure for a Setup Orientation

The previously defined measures can each aid in defining a good or bad setup orientation from all candidates; however, we desire an overall composite measure to drive toward an optimized set of setups.

For a given candidate setup orientation, we propose a quantitative goodness measure as defined by four variables, namely; 1) Toolpath Containment (TCO); 2) Toolpath Crossover (TCR); 3) Toolpath Redundancy (TR), and 4) Normal Deviation. While Normal Deviation simply is the difference between the candidate orientation and the average sub-surface normal, the other three variables are functions of Surface Visibility (SV) and Surface Reachability (SR) defined

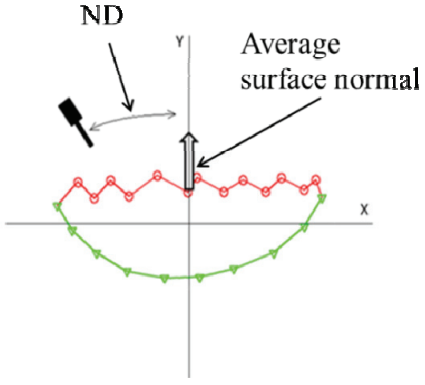

Figure 12: Normal Deviation between a candidate setup orientation and average surface normal

previously. The following presents each proposed variable used in the goodness calculations.

Toolpath Containment (TCO)

Toolpath Containment (TCO) is the idea of machining the visible and reachable sub-surface of primary interest. Since the overall goal is to choose the minimum number of setup orientations to machine a sub-surface, a setup orientation with maximum percentage TCO will always be chosen to machine the maximum sub-surface. For example, for machining a periosteal sub-surface (Figure 13) the setup orientation with maximum percentage of TCO of the periosteal sub-surface would be chosen.

$$TCO = \sum_{i=0}^{l}\sum_{j=0}^{m}\sum_{k=0}^{n}\left[(SV)_{i,j,k,p/a/f}\right] + \sum_{i=0}^{l}\sum_{j=0}^{m}\sum_{k=0}^{n}\left[(SR)_{i,j,k,p/a/f}\right]$$

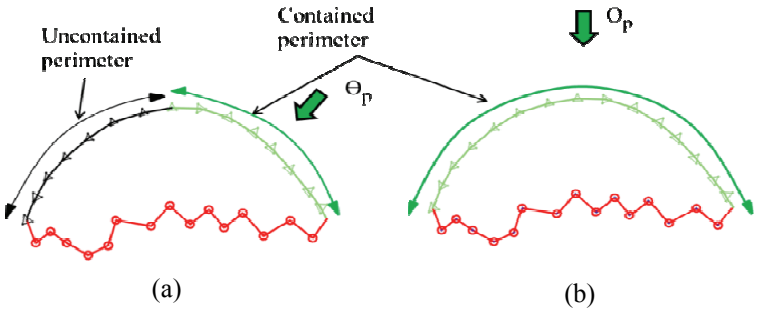

Figure 13: Toolpath Containment a) Partial Surface contained by an orientation b) Complete Surface contained by an orientation

Toolpath Crossover (TCR)

Toolpath Crossover (TCR) occurs if the machining is performed using a setup orientation(s) from which unintentional sub-surfaces are covered in addition to the sub-surface of primary interest (Figure 14). For example, TCR from the periosteal to fracture sub-surface means that both these sub-surfaces are machined when the intention was to machine only the periosteal sub-surface. TCR can have harmful effects on the implants functionality. For example, TCR from the periosteal to the fracture sub-surfaces can reduce the primary fixation stability of the implant. TCR from fracture to periosteal sub-surface would create a rough texture on the periosteal sub-surface, which could irritate the overlying soft tissues. Regardless, the goal is simple; machine each sub-surface with customized toolpaths, and avoid machining other sub-surfaces while doing so. Hence, the setup orientations giving *minimal* TCR are chosen for machining.

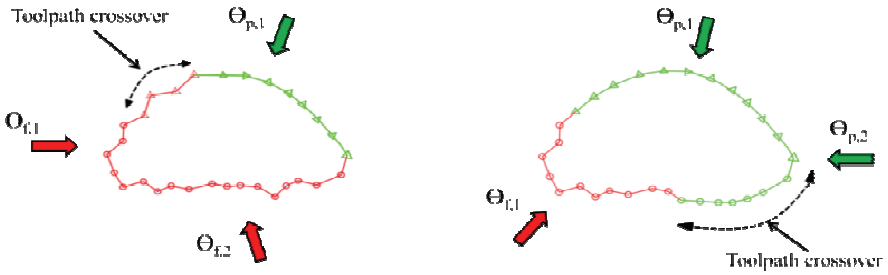

(a) (b)

Figure 14 - Toolpath Crossover (a) Fracture to Periosteal surface (b) Periosteal to Fracture surface

$$TCR = \sum_{i=0}^{l}\sum_{j=0}^{m}\sum_{k=0}^{n}\left[(SV)_{i,j,k,p/a/f}\right] + \sum_{i=0}^{l}\sum_{j=0}^{m}\sum_{k=0}^{n}\left[(SR)_{i,j,k,p/a/f}\right]$$

Toolpath Redundancy (TR)

Toolpath Redundancy (TR) is simply redundant machining of a common sub-surface perimeter reachable from multiple sub-surface-specific orientations (Figure 15). For example, Redundant machining on periosteal or articular sub-surface would just be inefficient, since additional smoothing of those sub-surfaces is insignificant. However the machining time could impact the practical use of this technology in a production setting (cost, machine capacity, etc.). Furthermore, redundant machining of fracture sub-surface could also reduce texturing effects (or ablate them completely). This would potentially lead to reduction in fixation stability of the implant. Hence, the setup orientations giving *minimal* TR are be chosen for machining.

$$TR = \left\{\sum_{=0}^{x}\left\{\sum_{i=0}^{l}\sum_{j=0}^{m}\sum_{k=0}^{n}\left[(SV)_{i,j,k,p/a/f}\right] + \sum_{i=0}^{l}\sum_{j=0}^{m}\sum_{k=0}^{n}\left[(SR)_{i,j,k,p/a/f}\right]\right\} - 100\right\}$$

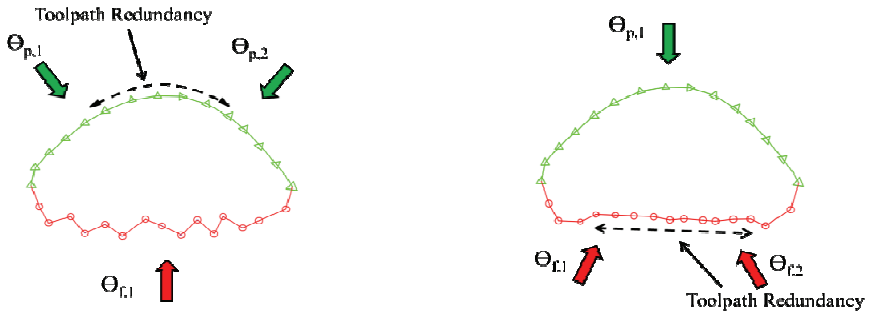

(a) (b)

Figure 15: Toolpath Redundancy a) Periosteal surface b) Fracture surface

Multi-objective function using Greedy Heuristic

Based on the previously presented measures, a multi-objective function is proposed that aids in choosing setup orientations that; 1) *maximize* Toolpath Containment (*Max* TCO), 2) *minimize* Toolpath Crossover on to the undesired sub-surfaces (*Min* TCO), 3) *minimize* Tool Path Redundancy (*Min* TCR), and 4) *minimize* the Normal Deviation for the targeted sub-surface (*Min* ND). The simple objective function is as follows:

$$Max\ \{\alpha[\mathrm{TCO}] - \beta[\mathrm{TCR}] - \lambda[\mathrm{TR}] - \delta[\mathrm{ND}]\}$$

In addition to the previous implementation of an algorithm to solve for the setup angles, this multi-objective function is now used to evaluate the "goodness" score of a feasible solution. The score is evaluated for each candidate orientation within 0°-359° range about the chosen axis of rotation. A feasible solution is a set of setup orientations that will solve the set cover problem and that will allow machining of the entire implant with customized sub-surfaces. Iteration is performed among a series of feasible solutions, taking the solution that maximizes the objective function. Under the assumption that only three types of sub-surfaces exist on an implant, the problem can be tightly bound to a limited set of feasible and likely solutions; hence, a semi-exhaustive search can be practically used. As an example, Figure 16 shows a plot of the normalized objective function score versus the setup orientations for the fracture sub-surface. The setup orientation corresponding to the maximum objective function score is the best orientation that can be used for creating the textured sub-surface.

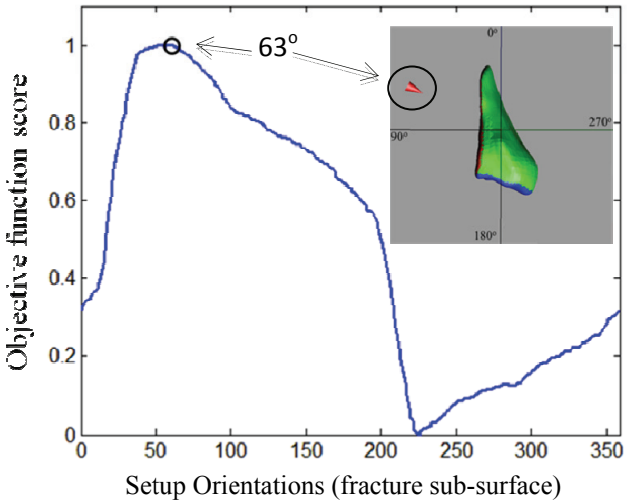

Figure 16: Normalized score vs. Fracture sub-surface specific orientations (Red pointer-optimal orientation)

Implementation

In summary, the machining of harvested implants with density gradients similar to that of the original bone should provide better bone in-growth rate and better strength to the load bearing implant. Additionally the customized sub-surface roughness helps to increase the implant's initial fixation stability and maintains its biomechanical compatibility. It is hypothesized that this will reduce healing time in the short term and reduce the likelihood of longer term issues like PTOA. The algorithms for determining the implant harvesting site and sub-surface specific setup orientations were implemented in computer software using C++ and are presented as follows.

Harvesting software implementation

The algorithms developed in this work have been implemented in C++ and are graphically displayed using *OpenGL*. To illustrate the implementation of these analyses, two sets of human tibia bone CT scan slices are used. These slices were first imported into ITKsnap (open source software) and saved as a voxel array DICOM file. Next, the DICOM data were loaded into Matlab, and the five Matyroshka shells were generated. The created shells were then saved into a .ply file in MATLAB, and imported to RapidForm software for post-processing. Post-processing included correcting geometric errors in the .ply file (holes, spikes, etc.). Results are presented in Figures 17-19, where Figure 17 shows the plots of similarity and density scoring quantitatively, Figure 18 graphically shows the harvesting site iteration process and finally, Figure 19 shows the machined implant harvested at an appropriate location in a donor bone surrogate (Sawbones® Distal Tibia).

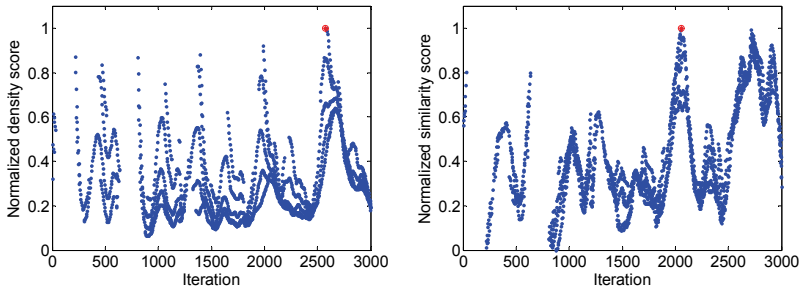

(a) (b)

Figure 17 - Plot of normalized density score (a) and similarity score (b)

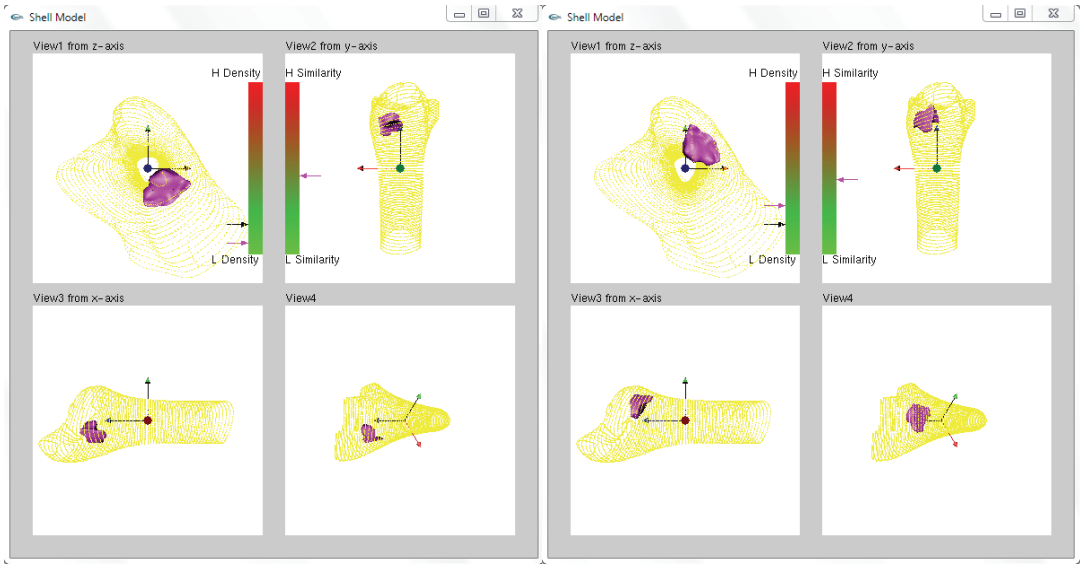

(a) (b)

Figure 18 - Implementation results for two provisional implant harvest sites. (a) Initial location of the implant within the donor bone; (b) The location of the implant is updated by rotating about the *Z*-axis by 103.5^{o}, translating along the *Z*-axis direction by -4.0 mm, and moving radially by 1.0 mm

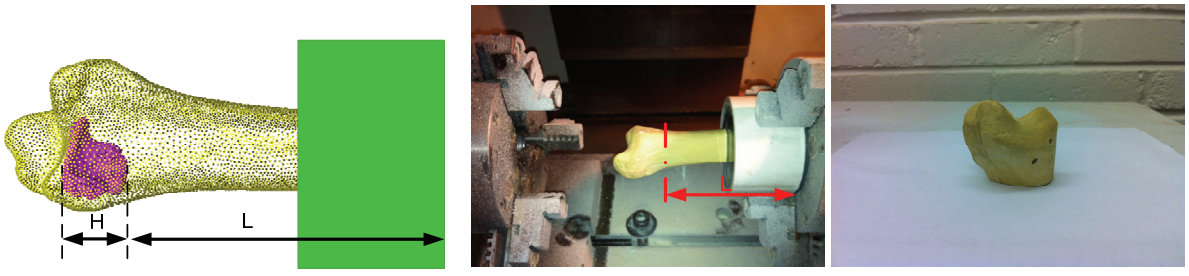

(a) (b) (c)

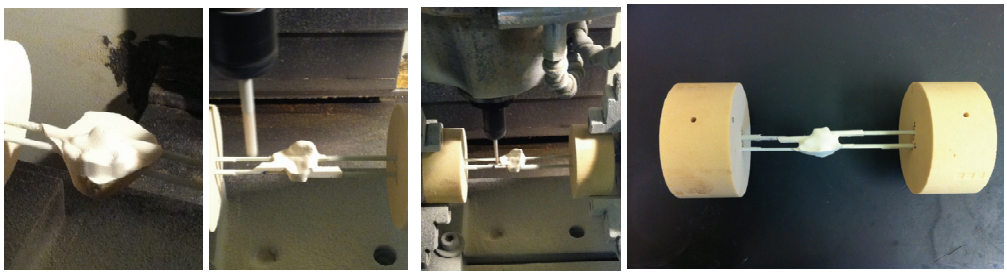

(d) (e) (f) (g)

Figure 19 - An example of implant harvesting using CNC-RP. (a) Harvested implant within the bone; (b) The potted bone is clamped in CNC milling machine; (c) Section cut of the bone; (d) Bone section with sacrificial supports, (e) Rough machining; (f) Finish milling; (g) Finished implant

Process Planning

The above-described algorithms for calculating sub-surface specific setup orientations were implemented in C++ and an OpenGL user interface, and were tested on an Intel Core2Duo, 2.8 GHz PC, and running Windows 7. The software accepts colored 2D slice files from 3D PLY models as input and output setup orientations necessary to machine the implants with customized surface roughness. Figure 20 shows setup orientations calculated for an implant, its OpenGL UI showing three orientations and the corresponding implant machined with the orientations illustrating the intended rough texture on the fracture sub-surface.

CNC-RP$_{bio}$ orientations	
Surface	Orientations
Fracture	84^0, 335^0
Periosteal	154^0
Articular	-

(a)

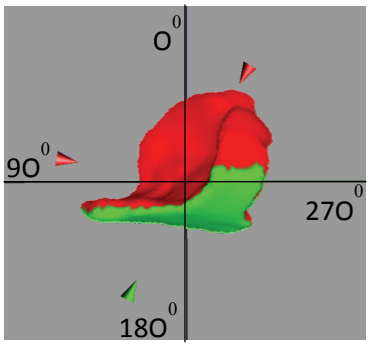

(b)

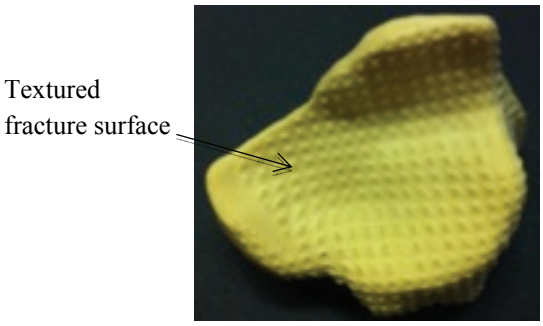

(c)

Figure 20 - Process Planning implementation (a) Setup orientations (b) Implemented UI (c) Machined implant

Conclusion & Future work

Harvesting

This paper presented a new method to represent multi-material models using nested polygonal shells, analogous to a Matryoshka stacking doll. Compared with the traditional way of hand-creating an assembly model, this method could potentially be completely automated, given a set of parameters. This work illustrates how the Matryoshka model can be used to plan harvesting locations for creating custom bone implants from within actual human donor bones, and it develops an approach to calculate a Density score and Similarity score for an arbitrary provisional implant harvest site, to evaluate the overall effectiveness of that harvest site. Future work with the Matryoshka approach could be to develop a better harvesting solution for irregular and/or flat bones with no proper axis definition. This method also could be used for industrial components which may have less amorphous shapes, and which could be printed using existing additive systems such as LENS or polyjet printing for objects with gradient material properties, for example.

Process Planning

Additionally this paper also introduces a new method for calculating setup orientations to create implants with customized surfaces. Texturing the fracture sub-surface could reduce implant/host bone interfacial movement and increase stability, while a smooth periosteal and articular sub-surfaces could enhance biomechanical compatibility. This technique for calculating setup orientation has the potential to produce implants with improved performance, and consequently to improve patient outcomes. The proposed algorithms could also be modified for industrial purposes such as in applications where the number and/or types of sub-surfaces present on the part may be more numerous, for example, when a variety of GD&T callouts are defined.

Acknowledgements

This work was supported by grants from the NIH/NIAMS (P50AR055533 and R21AR054015), the Roy J. Carver Charitable Trust at the University of Iowa, State of Iowa Economic Development appropriations to the Board of Regents under the Grow Iowa Values Fund, and the Musculoskeletal Transplant Foundation. The authors would also like to recognize the technical support of Mr. Gary Ohrt and Dr. Thad Thomas at the University of Iowa.

[1] Frank, M.C., Wysk, R.A., and Joshi, S.B. (2004), “Rapid Planning for CNC Machining – A New Approach to Rapid Prototyping”, *Journal of Manufacturing Systems*, SME, Vol. 23, No. 3, pp. 242-255.

[2] Frank, M.C., Hunt, C.V., Anderson, D.D., McKinley, T.O. and Brown, T.D. (2008), "Rapid manufacturing in biomedical materials: using subtractive rapid prototyping for bone replacement", *Proceedings of the Solid Freeform Fabrication Symposium*, August, Austin TX. pp. 686-696.

[3] Willis, A., Anderson, D., Thomas, T., Brown, T. and Marsh, J.L. (2007), "3D reconstruction of highly fragmented bone fractures". *Proceedings of the SPIE Conference on Medical Imaging*, Vol. 6512, pp.65121P1-65121P10.

[4] Thomas, T.P., Anderson, D.D., Willis, A.R., Lui, P., Frank, M.C., Marsh, J.L., Brown, T.D. (2011), “A computational/experimental platform for investigating three-dimensional puzzle solving of comminuted articular fractures.” *Computer Methods in Biomechanics and Biomedical Engineering*, Vol. 14, No. 3, pp. 263–270.

[5] Nauth A, McKee M.D., Einhorn T.A., Watson J.T., Li R, Schemitsch E.H. (2011). Managing bone defects. J Orthop Trauma. Vol. 25, No. 8, pp.462-466.

[6] Bosse M.J., MacKenzie E.J., Kellam J.F., Burgess A.R., Webb L.X., Swiontkowski M.F., Sanders R.W., Jones A.L., McAndrew M.P., Patterson B.M., McCarthy M.L., Travison T.G., Castillo R.C. (2002), An analysis of outcomes of reconstruction or amputation after leg-threatening injuries. New Engl J Med. Vol.347, pp.1924–1931.

[7] Vallier H.A., Hennessey T.A., Sontich J.K., Patterson B.M. (2006). Failure of LCP condylar plate fixation in the distal part of the femur - A report of six cases. J Bone Joint Surg Am. Vol.88, pp.846–853.

[8] Frank, M.C., Wysk, R.A., and Joshi, S.B. (2006), "Determining Setup Orientations from the Visibility of Slice Geometry for Rapid CNC Machining", *Journal of Manufacturing Science and Engineering, Transactions of the ASME*, Vol. 128, No. 1, pp. 228-238.

[9] Frank, M.C. (2007), "Implementing Rapid Prototyping Using CNC Machining (CNC-RP) Through a CAD/CAM Interface", *Proceedings of the Solid Freeform Fabrication Symposium*.

[10] Li, Y. and Frank, M.C., (2007), "Computing Non-Visibility of Convex Polygonal Facets on the Surface of a Polyhedral CAD Model", *Computer Aided Design*, Vol. 39, No. 9, pp. 732-744.

[11] LI, Y. and Frank, M.C. (2006), "Machinability Analysis for 3-axis Flat End Milling", *Journal of Manufacturing Science and Engineering, Transactions of the ASME*, Vol. 128, No. 2, pp. 454-464.

[12] Boonsuk, W. and Frank, M.C. (2009), "Automated fixture design for a rapid machining process", *Rapid prototyping journal*. 15, No.2, pp. 111-125.